

***Ab initio* study of low-energy electronic collective excitations in bulk Pb: anisotropy and acoustic modes.**

X. Zubizarreta,^{1,2} V. M. Silkin,^{1,2,3} and E. V. Chulkov^{1,2,4}

¹*Donostia International Physics Center (DIPC), Paseo de Manuel Lardizabal 4,
20018 San Sebastián/Donostia, Basque Country, Spain*

²*Departamento de Física de Materiales, Facultad de Ciencias Químicas,
Universidad del País Vasco/Euskal Herriko Unibertsitatea,*

Apdo. 1072, 20080 San Sebastián/Donostia, Basque Country, Spain

³*IKERBASQUE, Basque Foundation for Science, 48011 Bilbao, Spain*

⁴*Centro de Física de Materiales CFM - Materials Physics Center MPC,
Centro Mixto CSIC-UPV/EHU, Paseo de Manuel Lardizabal 5,
20018 San Sebastián/Donostia, Basque Country, Spain*

(Dated: February 19, 2013)

A theoretical study of the dynamical dielectric response of bulk lead at low energies is presented. The calculations are performed with full inclusion of the electron band structure calculated by means of a first-principles pseudopotential approach. The effect of including the spin-orbit splittings in the band structure is analyzed, together with dynamical exchange-correlation and local-field effects. Excitations are studied in detail, showing the presence at small momenta of acoustic-like dispersing excitations. The character of these modes with sound-like dispersion depends on the direction of the momentum transfer \mathbf{q} . In general results show strong anisotropy effects on the dielectric response of bulk Pb. Comparison with available optical experimental data shows good agreement.

PACS numbers: 71.20.Be, 71.45.Gm

I. INTRODUCTION

One of the characteristic of lead is that it presents the second-highest critical temperature of all bulk elemental superconductors ($T_c = 7.23$ K), which has been shown to be related to its large electron-phonon coupling (EPC) constant. In addition, spin-orbit (SO) coupling has a strong impact on the electron-phonon interaction in bulk Pb, increasing its strength as much as 44%.¹ Studying the electronic collective excitations near the Fermi level (E_F) and the SO effects on them would complete the description of low-energy dynamics in bulk lead, and it is done in the present work.

For many years the electron-density response of solids was studied using a free-electron gas (FEG) model in which the electron valence density is parametrized by a single quantity: the density parameter r_s , which stands for the average inter-electron distance.² The FEG model gave insight on basic properties of the momentum- and frequency-dependent dynamical dielectric response. However, band structure effects that are missing in a FEG model frequently produce dramatic impact on the dynamical dielectric response of solids. In particular, interband transitions (not present in a FEG model) give rise, for instance, to a strong red shift of the Ag plasmon frequency³ or to a negative momentum dispersion of the plasmon in Cs⁴. Additionally, interband peaks dominate the energy-loss landscape in the low-energy transfer regime. Also, it has been shown that band structure effects play an important role in the screening of charges at noble metal surfaces.⁵

For three-dimensional (3D) solids the FEG model predicts the existence of a r_s -dependent threshold for col-

lective excitations. Thus, according to the FEG theory, plasmons can not participate in the low-energy dynamical processes near the Fermi surface. However, Pines^{6,7} in the fifties predicted the existence of a very-low energy excitation, which should be present in systems with several energy bands crossing the Fermi level with different Fermi velocities (v_F), as it is the case of bulk Pb. This very-low energy mode presents an acoustic-like dispersion at small momenta: $\omega_{AP} = v \cdot q$, where v is the constant group velocity of the acoustic plasmon. Thus, ω_{AP} tends to zero as $q \rightarrow 0$. Exchange of acoustic plasmons have been suggested as a possible mechanism of electron pairing in superconductors (see, i.e., Ref 8 and references therein). Nevertheless, to the best of our knowledge this kind of acoustic excitations has not been shown to exist experimentally. Very recently detailed *ab initio* calculations of the dynamical dielectric response of bulk MgB₂^{9,10} and Pd¹¹ predicted the existence of acoustic plasmons. In particular, in the case of Pd this acoustic mode presents a 3D character as it is found in all three high-symmetry directions.¹¹

The main aim of the present study is twofold. First, the complexity of the low-energy electronic response of bulk Pb is shown, together with the effect of the different physical ingredients. Second, the results on the acoustic modes are presented and analyzed in detail. Low-energy collective excitations show a strong anisotropic character. The calculations of the low-energy collective excitations have been done using the first-principles pseudopotential approach within the time-dependent density functional theory (TDDFT).^{12,13}

The rest of the paper is organized as follows: In Sec. II the details of the *ab initio* calculations of the dynam-

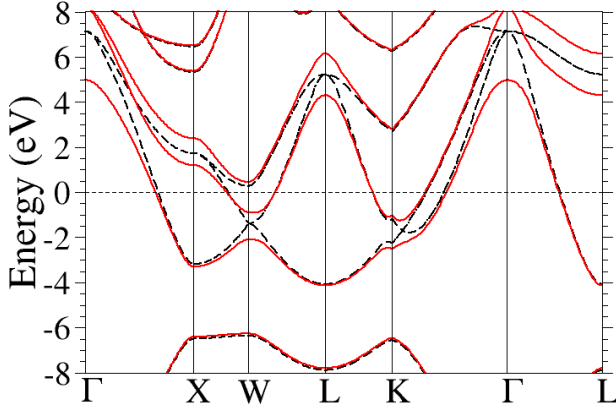


FIG. 1: (Color online) Calculated band structure of bulk lead, with (solid lines) and without (dashed lines) spin-orbit coupling in the Hamiltonian. The horizontal dashed line represents the Fermi level.

ical dielectric response of 3D solids are presented. In Sec. III the general results for the low-energy regime are presented together with comparison with experimental optical data, while in Sec. IV. the acoustic-like excitations are analyzed in detail. Finally, the main conclusions are presented in Sec. V. Unless otherwise stated, atomic units are used throughout, i.e., $e^2 = \hbar = m_e = 1$.

II. CALCULATION METHOD

A crucial quantity in the study of the dynamical dielectric response of solids is the dynamical structure factor $S(\mathbf{q}, \omega)$ as, within the first Born approximation, the inelastic scattering cross section of X-rays and electrons is proportional to it. $S(\mathbf{q}, \omega)$ is related by the fluctuation-

dissipation theorem to the dielectric function $\varepsilon(\mathbf{r}, \mathbf{r}', \omega)$. For a periodic solid,

$$S(\mathbf{q}, \omega) = -\frac{\Omega q^2}{2\pi} \text{Im}[\varepsilon_{\mathbf{G}=0, \mathbf{G}'=0}^{-1}(\mathbf{q}, \omega)] \quad , \quad (1)$$

where Ω is the normalization volume, \mathbf{G} 's are reciprocal space vectors, and $\text{Im}[\varepsilon_{\mathbf{G}=0, \mathbf{G}'=0}^{-1}(\mathbf{q}, \omega)]$ is the so-called energy-loss function, whose Fourier coefficients are related to those of the density-response function $\chi(\mathbf{r}, \mathbf{r}', \omega)$ through

$$\varepsilon_{\mathbf{G}, \mathbf{G}'}^{-1}(\mathbf{q}, \omega) = \delta_{\mathbf{G}, \mathbf{G}'} + v_{\mathbf{G}}(\mathbf{q}) \chi_{\mathbf{G}, \mathbf{G}'}(\mathbf{q}, \omega) \quad , \quad (2)$$

where $v_{\mathbf{G}}(\mathbf{q}) = \frac{4\pi}{|\mathbf{q} + \mathbf{G}|^2}$ is the Fourier transform of the Coulomb interaction.

The key quantity in the evaluation of Eq. (2) is the density-response function, which in the framework of TDDFT^{12,13} satisfies the matrix equation

$$\begin{aligned} \chi_{\mathbf{G}, \mathbf{G}'}(\mathbf{q}, \omega) &= \chi_{\mathbf{G}, \mathbf{G}'}^0(\mathbf{q}, \omega) + \sum_{\mathbf{G}''} \sum_{\mathbf{G}'''} \chi_{\mathbf{G}, \mathbf{G}''}^0(\mathbf{q}, \omega) \\ &\times [v_{\mathbf{G}''}(\mathbf{q}) \delta_{\mathbf{G}'', \mathbf{G}'''} + K_{\mathbf{G}'', \mathbf{G}'''}(\mathbf{q})] \chi_{\mathbf{G}''', \mathbf{G}'}(\mathbf{q}, \omega), \end{aligned} \quad (3)$$

where $\chi_{\mathbf{G}, \mathbf{G}'}^0(\mathbf{q}, \omega)$ are the Fourier coefficients of the density-response function of noninteracting Kohn-Sham electrons. $K_{\mathbf{G}, \mathbf{G}'}(\mathbf{q})$ stands for the Fourier components of the exchange-correlation kernel, whose exact form is unknown. Thus, approximations have to be used to describe $K_{\mathbf{G}, \mathbf{G}'}(\mathbf{q})$.

Instead of directly calculating $\chi_{\mathbf{G}, \mathbf{G}'}^0(\mathbf{q}, \omega)$, we calculate first the spectral function matrix $S_{\mathbf{G}, \mathbf{G}'}^0(\mathbf{q}, \omega)$ ^{14,15}

$$S_{\mathbf{G}, \mathbf{G}'}^0(\mathbf{q}, \omega) = \frac{2}{\Omega} \sum_{\mathbf{k}} \sum_n^{\text{occ}} \sum_{n'}^{\text{unocc}} \langle \psi_{n\mathbf{k}} | e^{-i(\mathbf{q}+\mathbf{G})\cdot\mathbf{r}} | \psi_{n'\mathbf{k}+\mathbf{q}} \rangle \langle \psi_{n'\mathbf{k}+\mathbf{q}} | e^{i(\mathbf{q}+\mathbf{G}')\cdot\mathbf{r}} | \psi_{n\mathbf{k}} \rangle \delta(\varepsilon_{n\mathbf{k}} - \varepsilon_{n'\mathbf{k}+\mathbf{q}} + \omega) \quad . \quad (4)$$

In Eq. (4), the factor 2 accounts for the spin degeneracy, n and n' are band indexes, \mathbf{k} is in the first Brillouin zone (BZ) and $\varepsilon_{n\mathbf{k}}$ and $\psi_{n\mathbf{k}}$ are Bloch eigenvalues and eigenfunctions, respectively, of the Kohn-Sham Hamiltonian. From the knowledge of $S_{\mathbf{G}, \mathbf{G}'}^0(\mathbf{q}, \omega)$, the imaginary part of $\chi_{\mathbf{G}, \mathbf{G}'}^0(\mathbf{q}, \omega)$ is easily evaluated using the expression

$$S_{\mathbf{G}, \mathbf{G}'}^0(\mathbf{q}, \omega) = -\frac{1}{\pi} \text{sgn}(\omega) \text{Im}[\chi_{\mathbf{G}, \mathbf{G}'}^0(\mathbf{q}, \omega)] \quad , \quad (5)$$

where $\text{sgn}(\omega) = 1$ (-1) for $\omega > 0$ ($\omega < 0$). The real part of $\chi_{\mathbf{G}, \mathbf{G}'}^0(\mathbf{q}, \omega)$ is obtained from the corresponding imaginary part using the Hilbert transformation.

For $\mathbf{G} \neq \mathbf{G}'$, the dielectric response couples the contri-

bution of $\mathbf{q} + \mathbf{G} \neq \mathbf{q} + \mathbf{G}'$ that appears as a consequence of the existence of variations of the electronic density in real solids, see Eq. (4). These couplings represent the so-called crystalline local-field effects (LFE). If LFE are neglected, the energy-loss function is simply given by

$$\begin{aligned} \frac{\text{Im}[\varepsilon_{\mathbf{G}=\mathbf{G}'=0}(\mathbf{q}, \omega)]}{|\varepsilon_{\mathbf{G}=\mathbf{G}'=0}(\mathbf{q}, \omega)|^2} &= \\ &= \frac{\text{Im}[\varepsilon_{\mathbf{G}=\mathbf{G}'=0}(\mathbf{q}, \omega)]}{\text{Re}[\varepsilon_{\mathbf{G}=\mathbf{G}'=0}(\mathbf{q}, \omega)]^2 + \text{Im}[\varepsilon_{\mathbf{G}=\mathbf{G}'=0}(\mathbf{q}, \omega)]^2}. \end{aligned} \quad (6)$$

For the density functional theory (DFT) ground state

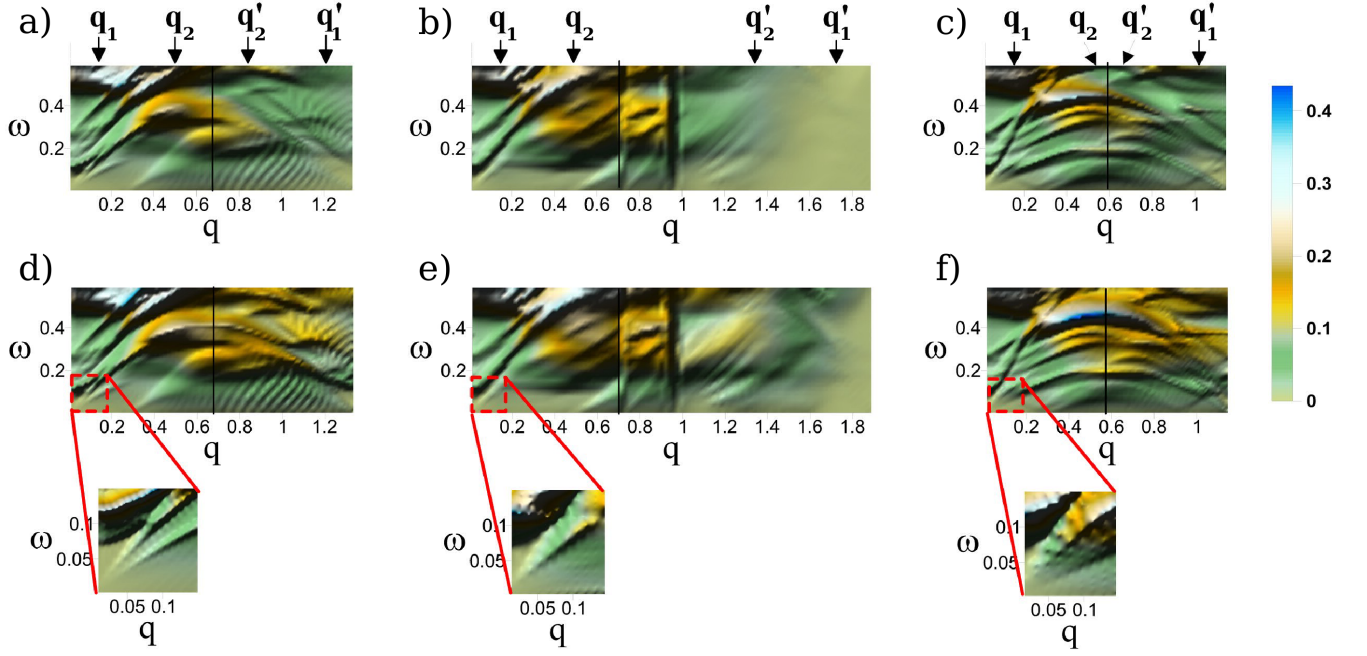


FIG. 2: (Color online) Energy-loss function surfaces for bulk Pb in arbitrary units, with (a),(d) \mathbf{q} along Γ -X, (b),(e) \mathbf{q} along Γ -K, (c),(f) \mathbf{q} along Γ -L. (a)-(c) are the results obtained neglecting LFE, while (d)-(f) include LFE. In all six plots, \mathbf{q} runs up to the Γ point of the corresponding second BZ. Vertical black lines mark $\mathbf{q}=\text{X,K,L}$. The colour bar applies for all the plots except the insets. For each high-symmetry direction, \mathbf{q}_1 , \mathbf{q}_2 , \mathbf{q}'_1 and \mathbf{q}'_2 mark the fixed values of the momentum transfer for which the energy-loss function is shown in Figs. 4-6. ω in Ry and $q=|\mathbf{q}|$ in Bohr^{-1} in all plots.

calculations, the electron-ion interaction is represented by norm-conserving non-local pseudopotentials,¹⁶ and the local density approximation (LDA) is chosen for the exchange and correlation potential, with the use of the Perdew-Zunger¹⁷ parametrization of the XC energy of Ceperley and Alder.¹⁸ Well-converged results have been found with a kinetic energy cut-off of 14 Rydberg (Ry), including ~ 150 plane-waves in the expansion of the Bloch states, for the face-centered cubic bulk Pb with the experimental lattice parameter $a = 4.95\text{\AA}$.

Two different sets of calculations were carried out in evaluating Eq. (4). First, $S_{\mathbf{G},\mathbf{G}'}^0(\mathbf{q},\omega)$ was calculated in the range $0 < \omega < 80$ eV with a step of $\Delta\omega = 0.04$ eV, the band indexes in Eq. (4) running up to $n = 25$. A Monkhorst Pack $144 \times 144 \times 144$ grid of \mathbf{k} vectors was used as the Brillouin zone sampling with ≈ 32000 vectors in the irreducible BZ (IBZ). The delta function was represented by a Gaussian of width 0.05 eV. Second, Eq. (4) was evaluated for very-low energies, in the range $0 < \omega < 4$ eV, with a step $\Delta\omega = 1$ meV, summing up to 12 bands. In this second set of calculations a finer $432 \times 432 \times 432$ grid was used, with ≈ 850000 \mathbf{k} vectors in the IBZ, and the width of the Gaussian replacing the delta function was 2 meV.

In Fig. 1 the calculated band structure along high-symmetry lines of the first BZ of bulk fcc lead is shown, including (solid lines) and excluding (dashed lines) the spin-orbit interaction in the Hamiltonian of the sys-

tem. As the fcc is centrosymmetric, due to the Kramers degeneracy¹⁹ each band is double-degenerated in both cases. The calculated band structure is in good agreement with other theoretical references (see, i.e., Ref.20) and with the experimental one²¹ when the SO term is taken into account. As can be seen in Fig. 1, the inclusion of the SO interaction has sizeable effects on the bands crossing the Fermi level (of p -orbital character), mainly around the high-symmetry reciprocal-space points. Thus, SO effects on the band structure of bulk Pb are expected to show up on its low-energy dielectric properties, see Fig. 3.

In the present work, in the band structure calculations the Hamiltonian including the SO term was solved fully self consistently. Then, in calculating $S_{\mathbf{G},\mathbf{G}'}^0(\mathbf{q},\omega)$ SO coupling enters Eq. (4) only through the energy spectrum via the δ function. The coupling matrices (the brackets in Eq. (4)) are kept the same (the ones with the wavefunctions calculated at the scalar-relativistic level) when using the scalar-relativistic energy spectrum or the one with the SO splittings included. Since SO-split bulk band structure of Pb, that possesses inversion symmetry, is reproduced in the first order perturbation theory,²² we only expect a weak modification of scalar-relativistic wave function by SO coupling. Therefore, we do not expect that the replacement of the spinor wave function by a scalar one should significantly modify the evaluated SO results.

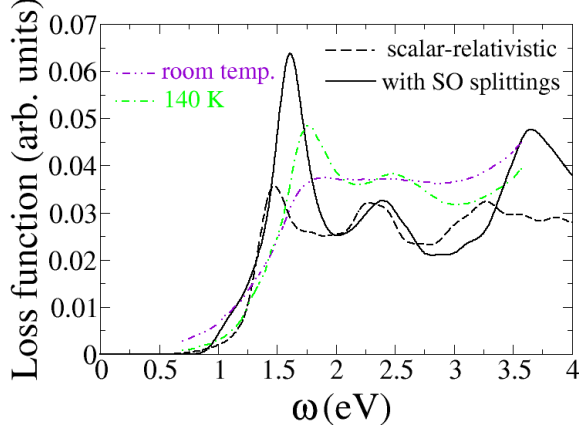


FIG. 3: (Color online) Comparison of calculated and experimental optical data. Theoretical results correspond to the smallest $\mathbf{q} \in \Gamma\text{-X}$, with $q=|\mathbf{q}| \simeq 0.009 \text{ Bohr}^{-1}$. LFE are included and the RPA is used. Experimental data at both temperatures from Ref. 24.

III. GENERAL RESULTS

The simplest estimation of the plasma frequency for a bulk metal is given by the FEG model as $\omega_p = \sqrt{4\pi n}$ with n being the electronic density, which in terms of the density parameter reads $\omega_p = \sqrt{3r_s^{-3}}$. For lead, using the experimental value of $r_s^{\text{exp}} = 2.298$, one gets $\omega_p^{\text{FEG}} = 13.53 \text{ eV}$. This theoretical value is in good agreement with the one obtained in electron energy-loss experiments, see references in Ref. 23. Thus, the energy transfer range $\omega \leq 8 \text{ eV}$ is well below the main bulk plasmon energy in bulk lead. Note also that calculating the dielectric response up to 80 eV the results are well converged with respect to the finite energy range used in the Hilbert transform.

In Figure 2 the energy-loss function surface $\text{Im}[\epsilon_{\mathbf{G}=\mathbf{G}'=0}^{-1}(\mathbf{q}, \omega)]$ calculated using the TDLDA approximation (see below) and including the SO-induced energy splittings is presented as a function of both the momentum transfer \mathbf{q} and energy transfer ω , with \mathbf{q} belonging to three different high-symmetry directions, both neglecting and including LFE. Note the strong anisotropic character of the dielectric screening. In all three directions of \mathbf{q} several peaks raised by interband and intraband transitions disperse. However, there are important differences. First, only for $\mathbf{q} \in \Gamma\text{-L}$ there is one well-defined interband peak, see Fig. 4. Second, the number of interband peaks is higher for $\mathbf{q} \in \Gamma\text{-L}$ than in the rest of the reciprocal space directions. Nevertheless, the main anisotropy effect is the distinct topology of the energy-loss function for $\mathbf{q} \in \Gamma\text{-K}$. The dispersion of the main interband peak is not flattened for \mathbf{q} in the BZ boundary. And interestingly, for \mathbf{q} vectors in the second BZ the dielectric response it is structureless, with no feature raising on top of a roughly flat background.

Comparison of the calculated energy-loss function with

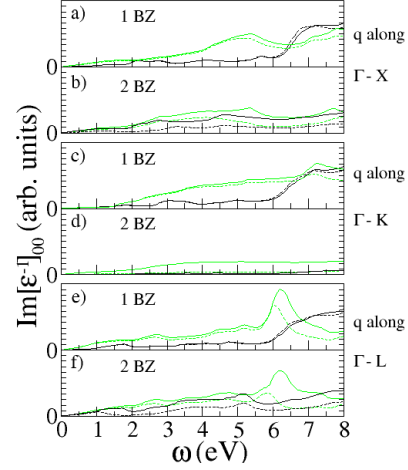


FIG. 4: (Color online) Fixed- \mathbf{q} $\text{Im}[\epsilon_{\mathbf{G}=0, \mathbf{G}'=0}^{-1}(\mathbf{q}, \omega)]$ curves. \mathbf{q} along $\Gamma\text{-X}$ in (a) and (b), along $\Gamma\text{-K}$ in (c) and (d), and along $\Gamma\text{-L}$ in (e) and (f). 1BZ and 2BZ stand for first BZ and second BZ results. Black lines correspond to \mathbf{q} close to the first or second BZ center [q_1 and q'_1 in Fig. 2 (a)-(c)], whereas light grey (green in online version) lines correspond to \mathbf{q} close to the BZ border [q_2 and q'_2 in Fig. 2 (a)-(c)]. Solid lines are results obtained with inclusion of LFE and SO-induced splittings at the TDLDA level (see text). Dashed curves are the corresponding results neglecting the LFE.

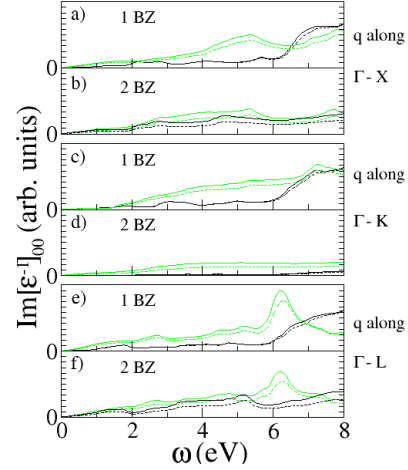


FIG. 5: (Color online) Same as Fig. 4, but with the dashed lines showing the energy-loss function calculated with inclusion of LFE and SO-induced splittings at the RPA level.

optical experimental data from Ref. 24 obtained at 140 K and room temperature is shown in Fig. 3. The calculated curves correspond to the smallest \mathbf{q} used along $\Gamma\text{-X}$, with $q=|\mathbf{q}| \simeq 0.009 \text{ Bohr}^{-1}$, allowing the comparison with optical experiments. As can be seen from the figure, including the SO-induced splittings in the band structure improves the overall agreement with the experiments, specially with the measurements carried at 140 K. The deviations of the energy transfer positions of the different features with respect to the experimental ones

decreases when including the SO-induced splittings in the calculation. However, the strong increase of the intensity of the interband peak at ~ 1.7 eV when including the SO splitting seems to worsen the agreement with the experimental measurements. Note that in the experimental data of Ref. 24 the two first peaks measured at $T=140$ K are washed out at room temperature. Thus, one expects the first interband peak to increase its intensity when measured at lower temperatures. This is in agreement with the fact that Pb presents a strong electron-phonon coupling, which should broaden the one-electron energy levels with increasing temperature. Then, taken into account that the methodology used in the present work applies for $T=0$ K, the conclusion is twofold: first, a satisfactory agreement with experiments is found which supports the approach used in the present work. Second, the comparison with the experimental optical data shows clear SO effects.

Below, a one-by-one systematic analysis of the effect of the main physical ingredients on the low-energy electronic collective excitations in bulk Pb is presented.

A. Local-field effects

As shown in Fig. 2, LFE affect differently the calculated dielectric response of bulk Pb depending on the direction of \mathbf{q} . As a common trend their effect is stronger for \mathbf{q} vectors in the second BZ. As can be seen from Fig. 4, neglecting LFE decreases the intensity of the energy-loss function for all three directions of \mathbf{q} , except for small q values (compare solid and dashed black lines in Fig. 4). More precisely, the two main effects of neglecting the LFE are washing out the strong structureless background for \mathbf{q} in the second BZ in Γ -K, and decreasing the intensity

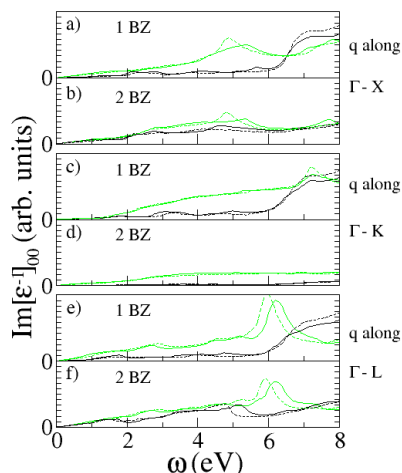


FIG. 6: (Color online) Same as Fig. 4, but with the dashed lines showing the energy-loss function calculated at the TDLDA level with inclusion of LFE and using the scalar-relativistic energy spectrum, without SO-induced band structure splittings.

of the main interband peak in Γ -L as q increases. The latter peak is shifted down in energy as much as 0.4 eV when neglecting the LFE.

B. XC kernel

When calculating the density-response function $\chi(\mathbf{r}, \mathbf{r}', \omega)$ of the interacting electrons from the knowledge of its non-interacting counterpart, short-range exchange and correlation (XC) effects are accounted for by the so-called exchange-correlation kernel, K^{XC} . The exact expression of K^{XC} is unknown, and one has to choose an approximation. Here, two different approaches are used for K^{XC} : the random-phase approximation (RPA) and the time-dependent local-density approximation (TDLDA)²⁵, an adiabatic extension of the local-density approximation. In the RPA one simply neglects the short-range exchange and correlation effects, thus, $K_{RPA}^{XC} = 0$.

In Fig. 5, the energy-loss function for several values of \mathbf{q} belonging to the three different high-symmetry directions is plotted, showing results obtained with both RPA and TDLDA. As can be seen, the effect of the TDLDA with respect to the RPA is the increase of the intensity of the calculated $\text{Im}[\epsilon_{\mathbf{G}=\mathbf{G}'}^{-1}(\mathbf{q}, \omega)]$, but without changing its shape. Only the main interband peak in Γ -L is slightly shifted down by ~ 0.1 - 0.2 eV, see Fig.5 (c).

C. SO-induced splittings effects

SO-induced energy band splittings also affect the dielectric response of bulk Pb in an anisotropic way. As shown in Fig. 6, in all three high-symmetry directions SO splittings lower the intensity of the broad feature at $\omega \geq 6$ eV. However, including the SO splittings in the calculation of the energy-loss function has sizeable effects for $\mathbf{q} \in \Gamma$ -X and Γ -L, but it is not the case for $\mathbf{q} \in \Gamma$ -K. In Γ -X, SO-induced band structure splittings broaden the scalar-relativistic interband plasmon around the first BZ border, shifting it to higher energies by as much as 0.7 eV. For $\mathbf{q} \in \Gamma$ -L, the main interband peak is shifted up in energy by ~ 0.4 eV upon inclusion of the SO splittings in the calculations.

IV. ACOUSTIC EXCITATIONS

In the insets of Fig. 2 (d)-(f) the energy-loss function for ($q \rightarrow 0$, $\omega \rightarrow 0$) is zoomed in. In all three directions of \mathbf{q} linear dispersing features which present vanishing energy transfer at vanishing momentum transfer appear. To study the exact character of these acoustic-like modes, highly detailed calculations are needed in order to resolve the thinnest details. Thus, results obtained using the second set of calculations (see Sec. II) are analyzed in the present section.

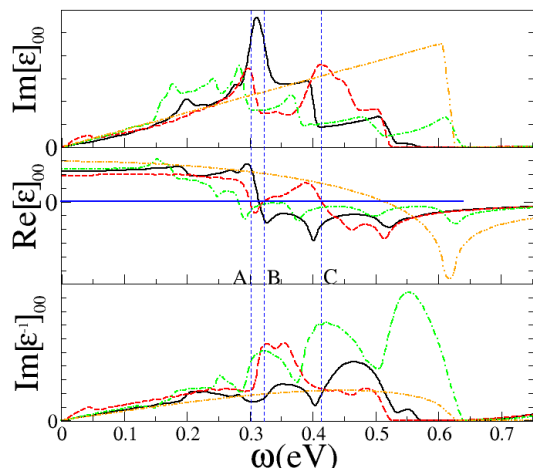


FIG. 7: (Color online) Imaginary and real part of the dielectric function of bulk Pb, as well as the corresponding energy-loss function. All curves correspond to the same $q=|\mathbf{q}| \simeq 0.027$ Bohr $^{-1}$, with $\mathbf{q} \in \Gamma$ -X (solid lines), $\mathbf{q} \in \Gamma$ -K (dashed lines) and $\mathbf{q} \in \Gamma$ -L (dashed-dotted lines). The dashed-dotted-dotted curves correspond to the Lindhard dielectric function for bulk Pb $r_s^{exp} = 2.298$. The vertical dashed lines (labeled A,B,C) mark values of ω where $\text{Re}[\epsilon]=0$ for \mathbf{q} along Γ -K (see text). All in arbitrary units.

As can be seen from the insets in Fig. 2, the acoustic modes in all three high-symmetry directions disperse keeping its character up to $q \simeq 0.14$ Bohr $^{-1}$ and $\omega \simeq 2$ eV ($\simeq 0.14$ Ryd in the units of ω in Fig. 2), when they get broaden out or merge with interband peaks. All modes also present a similar velocity of dispersion.

In Fig. 7, the calculated imaginary and real part of the dielectric function are presented, together with the corresponding energy-loss function with \mathbf{q} along all three different high-symmetry directions. The results were obtained including LFE, SO splittings and the TDLDA kernel in the calculations. The Lindhard dielectric function for $r_s^{exp} = 2.298$ and the energy-loss function derived from it are also shown (dotted lines). All curves correspond to $q=|\mathbf{q}| \simeq 0.027$ Bohr $^{-1}$. Comparison with the Lindhard screening (which stands for the dielectric response of a FEG) shows important band structure effects on the calculated $\epsilon(\mathbf{q}, \omega)$, which are responsible for the appearance of the acoustic modes.

As previously proven, in the range ($q \rightarrow 0$, $\omega \rightarrow 0$) neglecting LFE has little impact on the results (compare the black dashed and solid lines in Fig. 4). This allows for the analysis of the results shown in Fig. 7 to be based on the expression for the energy-loss function with no LFE, Eq. 6. Thus, if LFE can be neglected, peaks in the energy-loss function correspond to minima on both the real and imaginary parts of ϵ coinciding at the same (\mathbf{q}, ω) values. This is in constrast to the definition of plasmon in classical electrodynamics²⁶, which states that such collective excitations occur whenever $\text{Re}[\epsilon]=0$.

In Fig. 7 the dashed vertical lines mark the energy

transfer values at which $\text{Re}[\epsilon]=0$ for $\mathbf{q} \in \Gamma$ -K. As for the Lindhard screening case, there is one first $\text{Re}[\epsilon]=0$ crossing labeled by A, as in all the rest of curves. But only for \mathbf{q} along Γ -K $\text{Re}[\epsilon]$ crosses again zero, at B and C. At B, $\text{Im}[\epsilon]$ has a local minimum, whereas at C it presents a local maximum. As a consequence (see Eq. 6), at B a peak rises, which is not the case at C.

For $\mathbf{q} \in \Gamma$ -L, $\text{Re}[\epsilon]$ crosses zero only once, but it is close to vanish around ~ 0.35 eV, ~ 0.4 - 0.45 eV and ~ 0.55 - 0.6 eV. In all three cases, there is a local minimum in the imaginary part of the dielectric function. As a result, three peaks raise in the corresponding energy-loss function (see the green line in the lower panel of Fig. 7). However, from the point of view of classical electrodynamics, the character of the acoustics modes for \mathbf{q} along Γ -K and Γ -L are different as only in the former case the real part of the dielectric function vanishes several times in the very-low energy transfer range. This might reflect the fact that two and not only one band crosses the Fermi level in Γ -K, and thus be related to the acoustic plasmons (see the Introduction).

The v_F of the two bands crossing E_F along Γ -K are 14.6 eV·Bohr and 13.3 eV·Bohr. Comparing them with the group velocity of the acoustic plasmon in Γ -K, $v = 12.7(13.2)$ eV·Bohr including(excluding) SO coupling, one sees that v is comparable to the Fermi velocity of the bands. A detailed analysis of $\text{Im}[\epsilon]$ revealed that the acoustic plasmon is exclusively the result of the intra-band contributions of the two bands crossing E_F along Γ -K, as expected for $\text{Im}[\epsilon(q \rightarrow 0, \omega \rightarrow 0)]$.

The difference between the modes along Γ -K and along the rest of high-symmetry directions may not only be a matter of classification. Taking into account that the methodology used in the present work applies only at $T=0$ K, following the discussion of the comparison with experimental data (see Sec. III), at finite temperature one would expect the acoustic plasmon along Γ -K to be more suited than the modes along Γ -L for being resolved in electron energy-loss experiments. If the modes with $\mathbf{q} \in \Gamma$ -L broaden out, they would easily overlap with each other resulting in a highly broad feature. On the other hand, the well-defined acoustic plasmon in Γ -K presents a better background-peak intensity ratio and a smaller linewidth.

V. CONCLUSIONS

We have presented first-principles calculations of the low-energy ($\omega \leq 8$ eV) electronic collective excitations in bulk Pb and studied in detail the effect of the main physical ingredients involved, as well as the existence and character of acoustic-like modes. Good agreement with available optical experimental data is interpreted as an evidence of strong SO effects.

In general, strong anisotropic effects are found, results showing a distinct topology of $\text{Im}[\epsilon_{\mathbf{G}=0, \mathbf{G}'=0}^{-1}(\mathbf{q}, \omega)]$ for $\mathbf{q} \in \Gamma$ -K. LFE and SO-induced splittings have sizeable

effects on the dielectric screening of bulk Pb, showing an anisotropic behavior. For \mathbf{q} vectors in the second BZ, LFE on the energy-loss function are remarkable. Inclusion of exchange-correlation effects through the TDLDA kernel increases the intensity of the energy-loss function in the studied range, but without affecting its shape.

Very-low energy modes with acoustic-like dispersions are found in all three studied high-symmetry directions of \mathbf{q} and are shown to be a consequence of band structure effects. The character of these acoustic modes depends on the direction of \mathbf{q} . The possibility of experimental check of the existence of these acoustic modes by electron energy-loss measurements seems feasible as these modes keep their character up to $\omega \simeq 2$ eV. And as a result of a detailed analysis, the acoustic plasmon along Γ -K is suggested as the most suitable for its experimental detection.

As an overall conclusion, the present study has shown the complexity of the low-energy dielectric response of bulk Pb, even at the ($q \rightarrow 0$, $\omega \rightarrow 0$) limit through the anisotropic nature of the acoustic modes. Thus,

in theoretical studies of more complex properties (i.e., two-band superconductivity²⁷), care should be taken in using models for the dielectric properties of fcc bulk lead, the present results suggesting the need of an *ab initio* description²⁷ whenever possible. However, in an *ab initio* study on the inelastic lifetime of hot quasiparticles in bulk lead²⁸ -which presented agreement with experiments^{29,30}- no remarkable dependence on their momentum was found, with a small scattering of the calculated linewidths as a function of the quasiparticle energy (see Fig. 3 in Ref. 28).

ACKNOWLEDGEMENTS

We acknowledge financial support from the Spanish MICINN (No. FIS2010-19609-C02-01), the Departamento de Educación del Gobierno Vasco, and the University of the Basque Country (No. GIC07-IT-366-07).

-
- ¹ R. Heid, K.-P. Bohnen, I. Yu. Sklyadneva, and E. V. Chulkov, Phys. Rev. B **81**, 174527 (2010).
 - ² D. Pines and P. Nozières, *The Theory of Quantum Liquids* (Benjamin, New York, 1966).
 - ³ M. A. Cazalilla, J. S. Dolado, A. Rubio, and P. M. Echenique, Phys. Rev. B **61**, 8033 (2000).
 - ⁴ F. Aryasetiawan and K. Karlsson, Phys. Rev. Lett. **73**, 1679 (1994).
 - ⁵ R. Díez Muiño, D. Sánchez-Portal, V. M. Silkin, E. V. Chulkov, and P. M. Echenique, PNAS **108**, 971 (2011).
 - ⁶ D. Pines, Can. J. Phys. **34**, 1379 (1956).
 - ⁷ D. Pines and P. Nozières, Phys. Rev. **109**, 1062 (1958).
 - ⁸ Y. Ishii and J. Ruvalds, Phys. Rev. B **48**, 3455 (1993).
 - ⁹ V. M. Silkin, A. Balassis, P. M. Echenique, and E. V. Chulkov, Phys. Rev. B **80**, 054521 (2009).
 - ¹⁰ A. Balassis, E. V. Chulkov, P. M. Echenique, and V. M. Silkin, Phys. Rev. B **78**, 224502 (2008).
 - ¹¹ V. M. Silkin, I. P. Chernov, Yu. M. Koroteev, and E. V. Chulkov, Phys. Rev. B **80**, 245114 (2009).
 - ¹² E. Runge and E. K. U. Gross, Phys. Rev. Lett. **52**, 997 (1984).
 - ¹³ M. Petersilka, U. J. Gossmann, and E. K. U. Gross, Phys. Rev. Lett. **76**, 1212 (1996).
 - ¹⁴ F. Aryasetiawan and O. Gunnarsson, Phys. Rev. B **49**, 16214 (1994).
 - ¹⁵ F. Aryasetiawan, in *Strong Coulomb Correlations in Electronic Structure Calculations*, edited by V. I. Anisimov (Gordon and Beach, Singapore, 2001).
 - ¹⁶ G. B. Bachelet, D. R. Hamann, and M. Schlüter, Phys. Rev. B **26**, 4199 (1982).
 - ¹⁷ J. P. Perdew and A. Zunger, Phys. Rev. B **23**, 5048 (1981).
 - ¹⁸ D. M. Ceperley and B. J. Alder, Phys. Rev. Lett. **45**, 1196 (1980).
 - ¹⁹ M. Tinkam, *Group Theory and Quantum Mechanics* (McGraw-Hill, New York, 1971).
 - ²⁰ M. J. Verstraete, M. Torrent, F. Jollet, G. Zerah, and X. Gonze, Phys. Rev. B **78**, 045119 (2008).
 - ²¹ G. Jézéquel and I. Pollini, Phys. Rev. B **41**, 1327 (1990).
 - ²² E. V. Chulkov, Y. M. Koroteev, and V. M. Silkin, Surf. Sci. **247**, 115 (1991).
 - ²³ A. M. Ashton and G. W. Green, J. Phys. F: Metal Phys. **3**, 179 (1973).
 - ²⁴ A. G. Mathewson and H. P. Myers, Phys. Scr. **4**, 291 (1971).
 - ²⁵ E. K. U. Gross, J. F. Dobson, and M. Petersilka, in *Density Functional Theory II*, edited by R. F. Nalewajski (Springer, Berlin, 1996).
 - ²⁶ J. D. Jackson, *Classical Electrodynamics* (John Wiley & Sons, Inc., New York, 1999).
 - ²⁷ A. Floris, A. Sanna, S. Massidda, and E. K. U. Gross, Phys. Rev. B **75**, 054508 (2007).
 - ²⁸ X. Zubizarreta, V. M. Silkin, and E. V. Chulkov, Phys. Rev. B **84**, 115144 (2011).
 - ²⁹ I.-P. Hong, C. Brun, F. Patthey, I. Yu. Sklyadneva, X. Zubizarreta, R. Heid, V. M. Silkin, P. M. Echenique, K. P. Bohnen, E. V. Chulkov, and W.-D. Schneider, Phys. Rev. B **80**, 081409(R) (2009).
 - ³⁰ P. S. Kirchmann, L. Rettig, Z. Zubizarreta, V. M. Silkin, E. V. Chulkov, and U. Bovensiepen, Nat. Phys. **6**, 782 (2010).